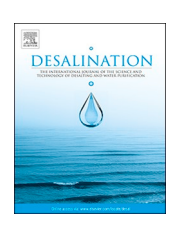


Contents lists available at ScienceDirect

Desalination

journal homepage: www.elsevier.com/locate/desal



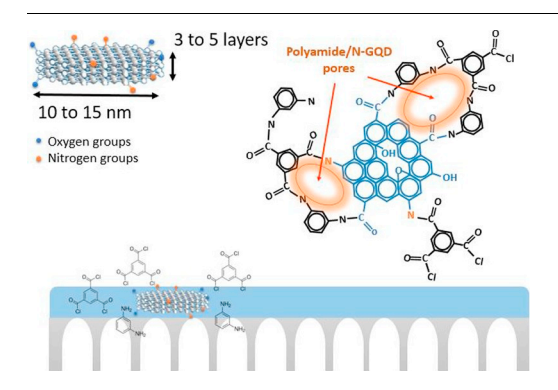
Polyamide/nitrogen-doped graphene oxide quantum dots (N-GOQD) thin film nanocomposite reverse osmosis membranes for high flux desalination



Mahdi Fathizadeh, Huynh Ngoc Tien, Konstantin Khivantsev, Zhuonan Song, Fanglei Zhou, Miao Yu*

Department of Chemical Engineering, SmartState Center of Catalysis for Renewable Fuels, University of South Carolina, Columbia, SC 29208, USA

GRAPHICAL ABSTRACT



ARTICLE INFO

Keywords: N-doped graphene oxide quantum dots Reverse osmosis Membrane Thin film nanocomposite

ABSTRACT

Thin film nanocomposite (TFN) has been shown as a promising platform to further increase water permeability of commercial polyamide membrane in reverse osmosis (RO) desalination. Identification of novel and effective nano-additives, which are significantly smaller than the typical thickness of polyamide membranes (~200 nm) and can be facilely incorporated into the interfacial polymerization (IP) process, is crucial to pursue this route. In this study, we prepared nitrogen-doped graphene oxide quantum dots (N-GOQD) and for the first time, fabricated polyamide/N-GOQD TFN membranes by IP for RO desalination application. We found adding only 0.02 wt/v% N-GOQD into polyamide membrane drastically increased water permeability by approximately 3 times, while maintaining similar salt rejection as the pristine polyamide membrane. Enhanced water permeability resulted from the improved hydrophilicity of the membrane surface, increased effective membrane surface area, and introduction of larger cavity at the interface between N-GOQD and PA matrix. In addition, favourable chemical bonding between polyamide and N-GOQD also greatly improved thermal stability of polyamide membrane, as indicated by thermal gravimetric analysis (TGA) measurements.

1. Introduction

Lack of clean and safe fresh water resources is a growing issue in modern world. Considering large fraction of sea water on the earth, sea water desalination, therefore, represents a viable solution to provide usable water for our daily life and industrial processes. Owing to its high-energy efficiency, reverse osmosis (RO) has become a more and more widely applied desalination technology [1–3]. Moreover, RO is

E-mail address: yumiao@cec.sc.edu (M. Yu).

^{*} Corresponding author.

simple to design and produces high quality clean water. Thin film composite (TFC) membranes are considered as the best RO membrane so far. The most used TFC membrane is the polyamide (PA) composite membrane fabricated by interfacial polymerization (IP) [4]. Currently, improving fouling and chlorine resistance and increasing water flux are the main focuses of developing PA TFC membrane to reduce operation cost and energy consumption [5].

Thin film nanocomposite (TFN) membranes based on PA have been prepared by adding inorganic nanoparticles, such as zeolites [6], titanium dioxide (TiO₂) [7], silicon dioxide (SiO₂) [8], functionalized carbon nanotubes [9], graphene oxide (GO) [10,11], and reduced GO (rGO) [12], into PA matrix during IP. These nanoparticles were found to facilitate water transport and thus enhance water flux, and also improve fouling and chlorine resistance. Typically, these nanoparticles are dispersed in either aqueous or organic phase, and subsequently participate in IP to form TFN membranes. Excellent dispersion of nanoparticles, therefore, is the crucial step to generate high quality TFN membranes. Identification of novel and effective nanoparticles, which are significantly smaller than the typical thickness of polyamide membranes (~100 nm) and can be very well dispersed in precursor solutions, is crucial to pursue this route.

Graphene oxide is an oxidized form of graphene that is made of carbon atoms bonded in hexagonal honeycomb lattice. Due to the strong oxidation conditions during its synthesis, for example, by Hummers or Staudenmaier method, a large number of oxygen-containing groups, including epoxide, hydroxyl, and carboxylic acid groups, exist on GO [13,14]. These functional groups lead to good hydrophilicity and allow excellent dispersion of GO flakes in water. So far, GO flakes have been deposited as ultrathin membranes with lamellar structure [15-17] or incorporated into various polymeric membranes for water purification ranging from microfiltration, ultrafiltration to nanofiltration [18-20]. Graphene oxide was also considered as a good candidate for making TFN PA membranes for RO desalination. Kim et al. [21] studied the effect of different GO loading in PA layer, and revealed that GO nanoparticles improved water flux and chlorine resistance. In a more recent study, loading GO flakes in PA membrane has been shown to increase water flux and improve organic fouling resistance during organic separation. Chae et al. [22] found that adding GO into PA increased water permeance from around 9 LMH to about 15 LMH at 225 psi feed pressure, and improved anti-bacterial properties by decreasing the amount of cells attached on the membrane surface. However, typical lateral size of GO flakes is in the range of several hundred nanometers, larger than the thickness of PA membranes. GO with much smaller sizes, therefore, is more favourable as an additive of TFN PA membranes to further improve its desalination performance.

Graphene oxide quantum dots (GOQD), with the diameter in the range of 3–20 nm, [23] have been applied in the anti-bacterial research field due to their unique properties, such as morphology, [24] ultrasmall lateral sizes, [25] and cytotoxicity [26] etc. GOQD, therefore may be an excellent candidate to replace GO in TFN PA membranes. Very few studies have been conducted on using GOQD in water purification membranes. Zeng et al. [27] employed GOQDs to fabricate a functionalized GOQD-PVDF membrane, and found improved hydrophilicity, anti-bacterial and anti-fouling performance. They showed that PVDF grafted with GOQD increased water flux from around 500 L/(m²-h·bar) to > 3800 L/(m²-h·bar) while improving antibacterial properties. Moreover, the hydrophilicity of PVDF membrane was significantly improved, and water contact angle dramatically decreased from 118.5° to 34.3° by coating GOQD on PVDF membrane surface.

In this study, we used a variant of GOQD, nitrogen-doped GOQD (N-GOQD), as a novel and effective additive to PA TFN membranes by taking advantage of its small lateral size (3–8 nm) and terminal amine groups that can form chemical bonding with PA matrix. We found that compared with PA membrane, PA TFN membranes had higher thermal stability, improved hydrophilicity, and higher effective surface area.

Optimized PA TFN membrane, therefore, showed a 3-time increase of water permeability while maintaining similar salt rejection.

2. Experimental

2.1. Chemicals and materials

Trimesoyl chloride (TMC) (98%), m-phenylenediamine (MPD) (flakes, 99%), n-hexane (laboratory reagent, \geq 95%), dichloromethane (anhydrous, \geq 99.8%, 40–150 ppm amylene as stabilizer), citric acid (99%), ammonia (28.0–30.0% NH $_3$ solution), and sodium chloride (NaCl, > 99%) were purchased from Sigma Aldrich and used without further purification. Polysulfone (PS) ultrafiltration membrane (P35, Nanostone Co., Minnesota, USA) was used as the support for PA and PA/N-GOQD TFN membranes.

2.2. Synthesis of N-GOQD

N-GOQD nanoparticles was synthesized by carbonization of citric acid with ammonia through hydrothermal treatment, following Zhan et al.'s method with some modification [28,29]. In brief, 80 mL citric acid aqueous solution (100 mg/mL) and 20 mL ammonia aqueous solution was transferred into a Teflon-lined autoclave and heated at $180\,^{\circ}\text{C}$ for 24 h. The light yellow resulting solution was dialyzed using a dialysis tubing (3000 Da, Spectrum Lab. Inc.) soaked in DI water for 4 h to remove impurities and excess ammonia. After dialysis, the aqueous dispersion was centrifuged at 10,000 rpm to remove any agglomerates. The supernatant was collected for subsequent membrane preparation, as described below.

2.3. Preparation of PA and PA TFN membranes

PA membrane was fabricated via IP on PS support. The PS support was taped on a glass plate and immersed in a MPD aqueous solution for 2 min. In this step, $100 \, \text{ml}$ of $2.0 \, \text{w/v}\%$ MPD solution in water was used and allowed to contact to PS membrane before draining the excess MPD solution. Then, excess aqueous MPD solution was removed from the PS support surface by a soft rubber roller. The rubber roller was firmly pressed over surface of PS membrane to ensure that no aqueous droplets on surface. After that, saturated PS support was soaked in a $100 \, \text{ml}$ of $0.1 \, \text{w/v}\%$ of TMC in n-hexane solution for $1 \, \text{min}$. The resulting membrane was washed by hexane for three times to remove unreacted monomers, cured at $60 \, ^{\circ}\text{C}$ for $6 \, \text{min}$. Finally, the fabricated membranes were stored in lightproof DI water bath at $5 \, ^{\circ}\text{C}$.

To prepare PA TFN membranes, MPD aqueous solution was replaced by aqueous solution of MPD and N-GOQD, and the membrane preparation procedure was the same as described above. N-GOQD aqueous solution with different concentrations was prepared by ultra-sonication. First, appropriate millilitre of 1 wt/v% N-GOQD aqueous solution was added to 50 ml DI water solution and sonicated for 1 h at room temperature. Then, N-GOQD solution mixed with 50 ml of 4.0 w/v% MPD solution to obtain the final solution with MPD concentration of 2.0 w/v% and N-GOQD concentration from 0 to 0.1 w/v% (Table 1).

2.4. Characterization of N-GOOQ and membranes

X-ray Photoelectron Spectroscopy (XPS) (Kratos Axis Ultra DLD instrument equipped with a monochromated Al Ka X-ray source and hemispherical analyzer capable of an energy resolution of 0.5 eV) and X-Ray Diffraction (XRD) (Rigaku D/Max 2100 Powder X-ray Diffractometer (Cu K α radiation)) measurements were conducted to characterize the elemental composition and structure of N-GOQD nanoparticles. The functional groups of membrane surface and N-GOQD nanoparticles were measured by Fourier Transform Infrared (FTIR) measurements in Attenuated Total Reflection (ATR) mode (Thermo Scientific, Waltham, MA, USA) with 4 cm $^{-1}$ resolution over a wave

Table 1
Summary of concentrations of MPD, TMC and N-GOQD in IP for preparation of different membranes.

Sample name	TMC (wt/v%)	MPD (wt/v%)	N-GOQD (wt/v%)
PA	0.1	2	0
PA0025	0.1	2	0.0025
PA005	0.1	2	0.005
PA01	0.1	2	0.01
PA02	0.1	2	0.02
PA04	0.1	2	0.04
PA07	0.1	2	0.07
PA10	0.1	2	0.1

number range of 600–4000 cm⁻¹. Particle size and distribution of N-GOQD was observed with transmission electron microscopy (TEM, JEM-2100F, JEOL Ltd. Japan) [29].

Field Emission Scanning Electron Microscope (FESEM) (Zeiss Ultra Plus) was used to observe the membrane morphology. Moreover, Atomic Force Microscopy (AFM) (TT-AFM, AFM workshop Co., CA, USA) was employed to analyze surface roughness in root mean square (RMS) and relative surface area of the fabricated PA layer. AFM images were taken over a membrane area of $5\times 5~\mu m^2$. Contact angle of water was measured by VCP Optima system (Optima XE) to compare the hydrophilicity of the fabricated membranes. Water droplets ($\sim 1~\mu L$) were dropped carefully onto the pristine PA and PA TFN membrane surface for imaging. All membrane samples were dried at ambient temperature prior to characterization.

Thermal gravimetric analysis (TGA) measurement was performed to investigate the thermal stability before and after adding N-GOQD in PA. To study specifically the thermal property of the PA and PA with N-GOQD, PS support with the top PA or PA with N-GOQD was firstly separated from the bottom nonwoven polyester. Then, PS support was dissolved in dichloromethane solution, and PA or PA with N-GOQD was collected from solution. Finally, TGA measurement was carried out under a nitrogen atmosphere using Perkin–Elmer thermo gravimeter (Diamond TG/DTA). The flow rate of nitrogen was 20 ml/min, and the heating rate was 10 °C/min from 25 to 700 °C.

2.5. Membrane permeation measurements

A stainless-steel dead-end module with an effective permeation area of $5.1~{\rm cm}^2$ was used for salt water permeation measurements (Fig. S1). Feed side was connected to a high-pressure nitrogen tank to generate a driving force around 15 bar. Desalination performance of PA and PA TFN membranes was evaluated using 2000 ppm NaCl solution at room temperature. An electronic scale (Ohaus, CS Series) was used to measure the mass of permeate over time (> 3 h), which was used to calculate the volumetric water permeance (J) at steady state. The salt rejection (R = 1 - C_p/C_f , where C_p and C_f are the salt concentration of permeate and feed, respectively) was calculated from the feed and permeate salt concentration. Concentration of NaCl was measured by a conductivity meter (Pour Grainger International, Lake Forest, IL, USA).

3. Results and discussion

3.1. N-GOQD characterization

TEM image (Fig. 1a) showed that the synthesized N-GOQD had a relatively uniform size distribution between 3 and 8 nm and were fully dispersed N-GOQD particles without apparent agglomeration. This is consistent with the finding by Zhang et al. [28] that N-GOQD particles do not react easily with each other and are stable in water at room temperature. In addition, most of N-GOQD particles are expected to contain a few nitrogen functionalized GO layers (3 to 5 layers) [29,30].

The AFM image and height profile of N-GOQD nanoparticles (Fig. 2S) confirmed that the synthesized N-GOQD particles have 1 to 5 GO layers.

As made N-GOQD showed carbon, oxygen and nitrogen signals at 283 to 290 eV, 530 to 533 eV and 398 to 402 eV in the XPS survey spectrum (Fig. S3a). Li et al. [31] found that the N1s XPS spectrum of N-GOQD can be fitted into two peaks (398 and 401 eV), which can be assigned to pyridinic at lower energy and amine or pyrrolic at higher energy. Fig. 1b indicates that N1s peak appeared at around 398-402 eV, confirming amine and pyridine groups of N-GOQD. Deconvolution of N1s peaks (Fig. S3b) revealed the signals of -NH₂ at 399.6 eV and N-C at 401.3 eV [32]. Oxygen-containing groups (O1s) generally contain several XPS spectrum peaks at 531.2 eV, 532.8 eV, and 535.4 eV for carboxylic acid, epoxy and hydroxyl groups, respectively [33]. O1s peak at around 531 eV suggests that N-GOQD also has acid groups that may react with TMC and MPD during IP reaction. Fig. S3c showed that N-GOQDs had the binding energy peaks at 284.6 eV, 286.4 eV, 289.6 eV, and 289.5 eV attributing to C=C bonds, C-N bonds, C-O bonds (hydroxyl and epoxy), and O = C-OH (carboxyl), respectively. The calculated ratios of N/C, O/C and H/C from XPS spectrum are 0.43, 0.87 and 0.14, respectively.

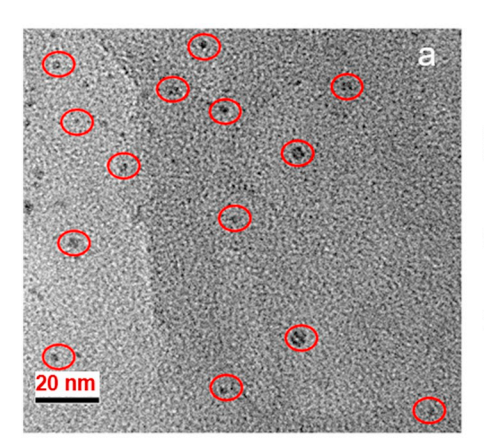
As observed in Fig. S4, the XRD pattern of N-GOQD showed a strong peak centered at 20.3°, corresponding to a d-spacing of around 4.2 Å. FTIR spectrum of N-GOQD in water was shown in Fig. 1b. Peaks at 1709 and 1790 cm⁻¹ for C=O stretch revealed the existence of the carboxylic group. Carboxylic group bonded with aromatic ring has FTIR peaks in the range of 1700 to 1730 cm⁻¹, and is expected to shift to higher wave numbers by replacing carbon with nitrogen in the aromatic ring [34]. Moreover, FTIR spectrum indicated the existence of C-H (1395 cm⁻¹), N-H stretch of amine group (1560 cm⁻¹), C=C (1450 cm⁻¹) and C-N (1060 cm⁻¹) groups in N-GOQD. FTIR spectrum also exhibited two distinct peaks associated with oxygen functional groups at 1208 cm⁻¹ (C-O stretching vibrations of epoxy) and 1670 cm⁻¹ (C=N stretching vibrations of pyrrolic structure). FTIR result of N-GOQD, therefore, is in a good agreement with that of the XPS spectrum.

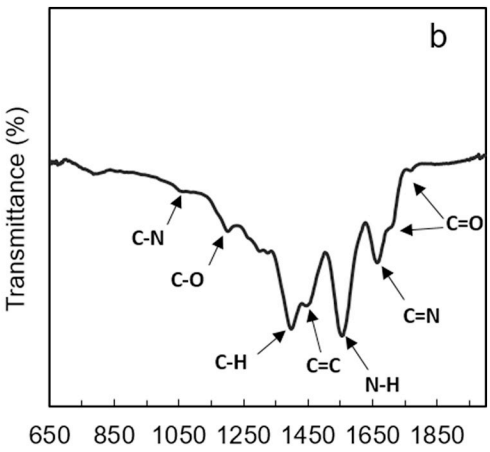
3.2. Membrane characterization

3.2.1. Membrane FESEM, ATR, TGA, AFM and contact angle characterization

Fig. 2 showed the FESEM images of the surface and cross section of PA and PA TFN membranes. PS support (Fig. S5) had pores between 10 and 30 nm, which makes it suitable as RO membrane support [1,4]. Surface images clearly indicated that adding N-GOQD nanoparticles changed the leaf-like morphology of PA membrane to hill and valley morphology of PA TFN, and higher N-GOQD concentration led to smoother surface (Fig. 2a, b and c). Adding different nanoparticles, such as zeolite, CNT, TiO₂, SiO₂ etc., into IP reaction has been found to better release the heat of reaction and thus improve surface roughness [35–38]. Apparently, addition of N-GOQD also facilitates heat release during IP and thus leads to smoother surface. Cross sectional view of PA, PAO2, and PAO7 (Fig. 2d, e, and f) showed an average skin layer thickness of around 250 nm in samples, suggesting N-GOQD had negligible effect on membrane thickness.

To further characterize the surface properties of PA TFN membranes prepared using different N-GOQD concentrations, we conducted AFM and water contact angle (CA) measurements. N-GOQD nanoparticles have various functional groups, such as carboxylic, amine, etc. (Fig. 1b and d), and thus are expected to participate in the IP reaction. With the increase of N-GOQD concentration in the precursor solution, surface roughness of PA TFN membranes first decreased and then increased slightly (Table 2); the minimum roughness was found for PA02 membrane. As shown in Fig. S6, by adding 0.02 wt/v% N-GOQD in the IP reaction, membrane surface morphology changed from low-density large bumps to high-density small bumps, which leads to a 1.5 time increase of the effective surface area (Table 2). Adding more N-GOQD





Wave number (cm⁻¹)

Fig. 1. a) TEM image and b) FTIR spectrum of N-GOOD.

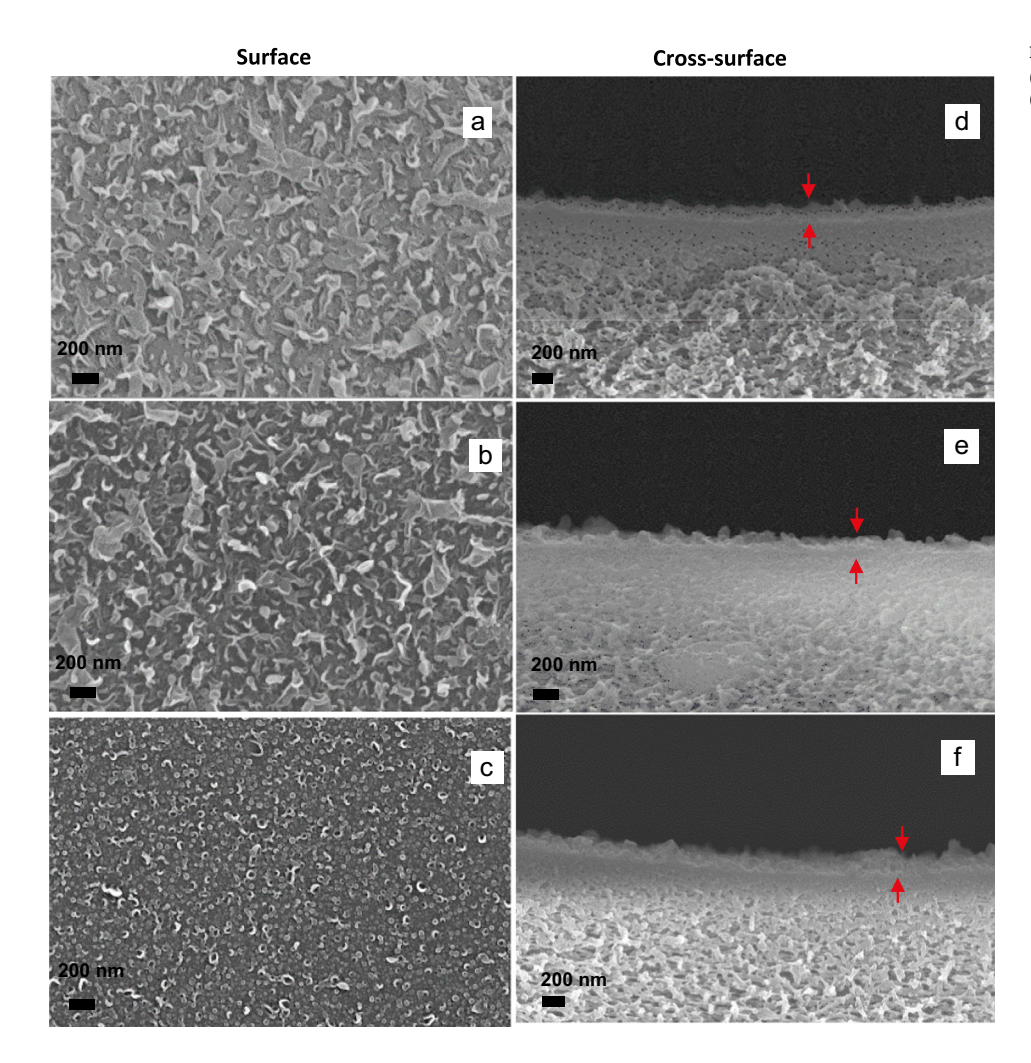


Fig. 2. FESEM images of the surface of PA (a), PA02 (b) and PA07 (c) and cross-section of PA (d), PA02 (e), and PA07 (f).

(PA07 and PA10), however, resulted in significantly reduced effective area, which is comparable to that of PA. This may result from the aggregation of N-GOQD nanoparticles. Several recent studies found that adding high concentration of nanoparticles to PA layer increased surface roughness because of nanoparticles agglomeration on membrane surface [37,39,40]. Adding N-GOQD into PA matrix also greatly improved its hydrophilicity, as shown in Table 2. CA of water gradually

decreased from 87° to $<60^\circ$ by adding up to 0.1% N-GOQD in IP reaction. Enhanced effective surface area, combined with improved surface hydrophilicity, is expected to increase water absorption and thus increase water permeability [41]. PA TFN membrane with N-GOQD as the additive, therefore, is expected to have greatly increased water permeability.

The ATR-FTIR spectra of PA and PA TFN membranes were presented $\,$

Table 2 Surface roughness, effective surface area (over a scan area of 5 μ m \times 5 μ m), and contact angle (CA) of PA and PA TFN membranes.

Sample	Ra (nm)	Rms (nm)	Effective surface area (μm²)	CA (°)
PA	78 ± 5	97.3 ± 3	41.2	87 ± 2
PA0025	78.3 ± 2	96.9 ± 3	46.1	86 ± 1
PA005	77.3 ± 4	95.9 ± 3	47.1	82 ± 3
PA01	72 ± 2	91.8 ± 3	67.3	73 ± 2
PA02	51.9 ± 3	66.4 ± 3	63.5	57 ± 4
PA04	55.9 ± 4	71.4 ± 3	61.3	58 ± 3
PA07	56.2 ± 4	76.3 ± 4	44.7	56 ± 2
PA10	54.7 ± 6	73.9 ± 5	38.9	56 ± 2

in Fig. 3. The peaks at 1488 and 1245 cm $^{-1}$ correspond to CH $_3$ –C–CH $_3$ stretching and C–O–C stretching of PS support (Fig. S7). Absorption bands at 1600–1700 and 1700–1760 cm $^{-1}$ are usually responsible for C=O group of polyamide and ester groups, respectively [42,43]. The amide bands of fabricated PA active layer appeared at around 1660, 1640 and 1080 cm $^{-1}$ for C=O stretching of carboxylic, N–H stretching of amide, and C–N stretching, respectively. PA layer with N-GOQD nanoparticles had a very wide peak from 1600 to 1720 cm $^{-1}$, which can be deconvoluted into three peaks, 1624 cm $^{-1}$ (N–H of amide), around 1650 cm $^{-1}$ (C=O of carboxylic), and 1670 cm $^{-1}$ (C=N of pyrrolic). The ATR-FTIR spectrum of pristine PA did not show the presence of amine N–H group at wavenumber of 1560 cm $^{-1}$, while this peak can be clearly seen in the N-GOQD/PA composite membrane.

The intensity of amine N–H peak increased with the increase of N-GOQD concentration till 0.02 wt/v%, and then significantly decreased. This suggests that amine groups of N-GOQD significantly contribute in IP, instead of MPD monomers. Moreover, the intensity of ester C=O of carboxylic group (1740 cm $^{-1}$) increased with N-GOQD concentration, suggesting that high concentration of N-GOQD may impede reaction between MPD and TMC monomers and thus lower degree of PA crosslinking.

TGA measurements were conducted to understand the effect of N-GOQD on the thermal stability of PA TFN, as shown in Fig. 4. Two weight losses were seen for PA at temperatures starting at around 280 and 450 $^{\circ}$ C, which can be assigned to degradation of unreacted functional groups, such as amine and acid groups, and decomposition of PA polymer.

TGA curve of N-GOQD revealed that the decomposition of N-GOQD started at about 180 $^{\circ}$ C and had a relatively low and gradually decreasing rate over a wide temperature range up to 700 $^{\circ}$ C. The functional groups of N-GOQD, such as amine and hydroxyl etc., are more heat sensitive than those of PA [44], and thus they can be more easily

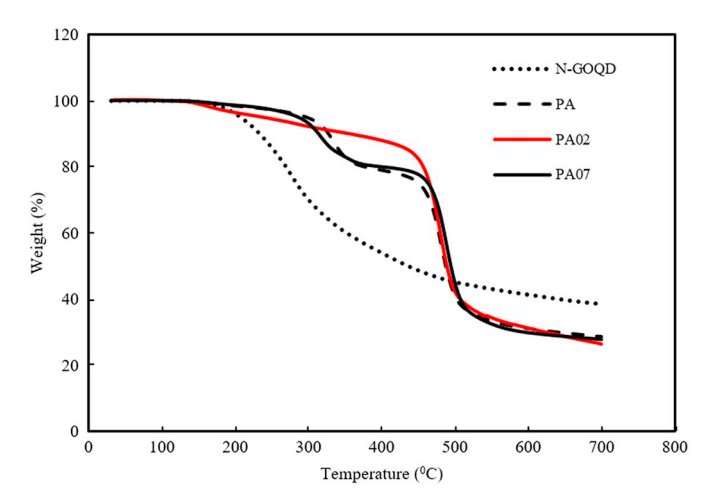
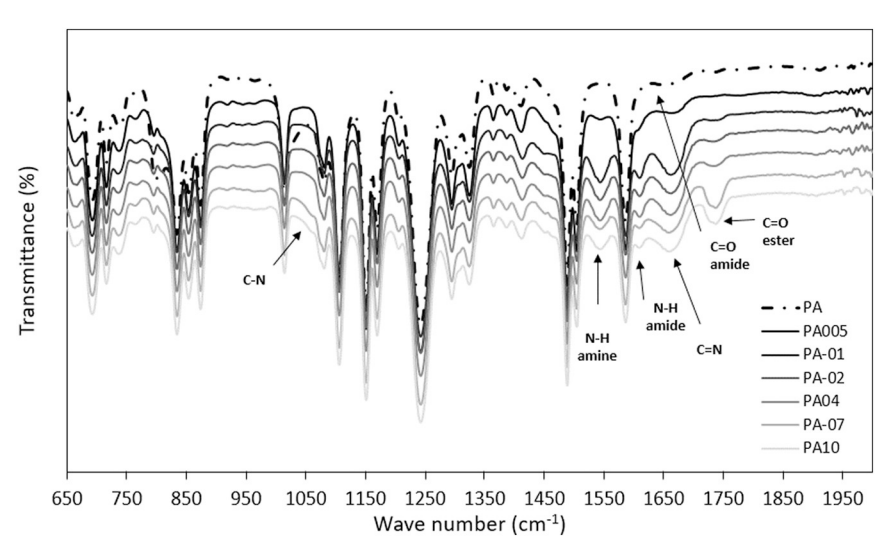


Fig. 4. TGA results of PA and N-GOQD/PA membranes.

removed from the N-GOQD surface. Decomposition of PA02 started at roughly the same temperature as that of N-GOQD, and only one major mass loss can be seen starting from 440 °C, following the similar trend as the second major mass loss of PA. Apparently, adding N-GOQD significantly improved thermal stability of the PA TFN. This may result from the participation of N-GOQD in the polymerization process, which leads to better cross-linked PA matrix and/or less residual/unreacted functional groups. However, PA07 with higher N-GOQD loading showed slightly higher decomposition rate than that of PA during the first major mass loss and almost the same rate during the second major mass loss. This suggests that adding too much N-GOQD might decrease the degree of PA crosslinking, which is consistent with the ATR-FTIR results (Fig. 3).

3.2.2. Desalination performance of PA TFN membranes

Desalination performance of PA TFN membranes was evaluated and compared with PA membrane, as shown in Fig. 5a. Water permeability of PA TFN membranes increased approximately linearly from 0.62 to 1.66 L/(m²-h·bar) with the increase of N-GOQD concentration from 0 to 0.02 wt/v% without sacrificing salt rejection (~93%). Further increasing N-GOQD concentration to 0.04 wt/v% had negligible effect on water permeability and salt rejection. Water permeability, however, decreased approximately linearly from 1.72 to 0.55 L/(m²-h·bar) with the increase of N-GOQD concentration from 0.04 to 0.1 wt/v%, whereas salt rejection decreased to 85% and 50% for 0.07 and 0.1 wt/v% N-GOQD, respectively.



 $\begin{tabular}{ll} Fig. & {\bf 3.} \ ATR\mbox{-}FTIR \ spectroscopy \ of PA \ and \ N\mbox{-}GOQD\mbox{/PA membranes}. \end{tabular}$

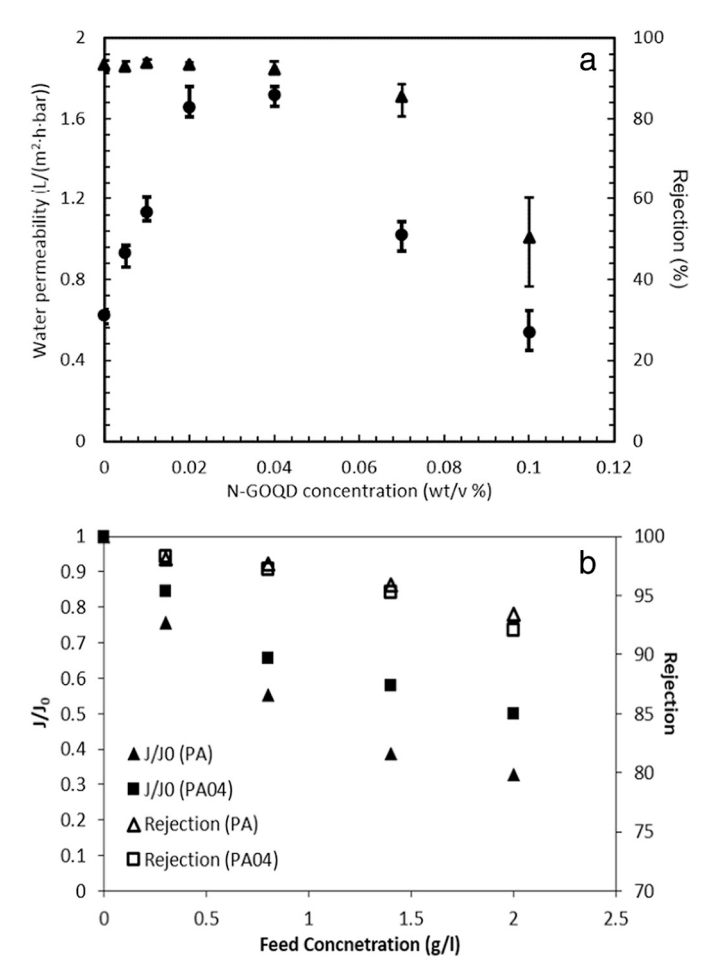


Fig. 5. a) Water flux and NaCl rejection of PA and N-GOQD/PA membranes (2000 ppm NaCl, 15 bar), and b) effect of feed concentration on PA TFC and PA04 TFN membrane ($J_0 = DI$ water permeability, J = salt/water permeability, 15 bar).

Favourable membrane surface properties, including high effective membrane area and excellent hydrophilicity, have been shown to increase water permeability during desalination [41,45]. Karan et al. [41] found that water permeability of PA membrane increased 4 times with the increase of the effective area by 1.8 times. Improved hydrophilicity is expected to increase water absorption and thus increase water permeability [46]. On the other hand, N-GOQD reacts with MPD and TMC monomers, as shown in Fig. 3, and cross-linking between N-GOQD and PA might create transport pathways with larger pores at the interface than those of PA matrix, due to the relatively sparse distribution of functional groups on N-GOQD. These larger pores are expected to facilitate water transport but may have lower salt rejection. Therefore, when N-GOQD loading in PA matrix is relatively low, existence of these larger interfacial pores may be beneficial for increasing water permeability. Considering both favourable surface properties (Table 2) and small amount of larger interfacial pores for PA0025 ~ PA04, water permeability increases while maintaining high salt rejection. For PA07 and PA10 with high N-GOQD loading, their effective surface area decreased significantly (Table 2) and became comparable to that of PA, whereas their CA of water was almost the same as that of PA04. Reduced effective surface area apparently greatly lowered water permeability.

Moreover, with high loading of N-GOQD in PA, it may crosslink with itself and agglomerate in the PA matrix, leading to local water blockage. Also, ATR results (Fig. 3) confirmed that high N-GOQD concentration caused change of polymer structure from polyamide to polyester, which can significantly decrease water flux and salt rejection [47]. Seman et al. [47] found that changing thin film structure of RO

membrane from polyamide to polyester decreased water permeability and salt rejection from 95% to < 60%. As an overall result of all these factors, PA TFN membranes (PA07 and PA10) with high N-GOQD loading exhibited both low water permeability and low salt rejection.

N-GOQD, therefore, has been shown as an effective additive for PA membrane to greatly improve its surface hydrophilicity and effective surface area, while introducing sparse large interfacial pores to facilitate water transport. Optimizing N-GOQD loading in PA matrix significantly increased water permeability without sacrificing salt rejection. Comparison between PA TFN membranes in this study with commercial PA TFC membrane indicates that TFN membranes with N-GOOD have better performance. Jeong et al. [35] found that the water permeability and NaCl rejection of SWHR (FilmTec Corp. Edina, MN) was $0.92 \pm 0.02 \, \text{L/(m}^2 \cdot \text{h·bar)}$ and 92%, respectively. We also selected PA TFC and PA04 TFN membrane for comparison. Our PA TFC membrane had water permeability of 0.72 L/(m²·h·bar) and salt rejection of 93.1%, which are very close to those of commercial PA TFC membrane. Adding 0.04 w/v% N-GOQD to PA layer (PA04 TFN membrane) increased water permeability to around 1.8 L/(m²·h·bar), which is 2 times higher than that of SWHR, but maintained similar NaCl rejection of 92.1%.

We selected a range of NaCl concentration from 0 to 2 g/l. Generally, osmotic pressure is a function of salt concentration in the feedwater. Increasing the salt concentration in feedwater decreases water permeance because of higher needed osmotic pressure. We studied the results of salt concentration for pure PA and PA TFN membrane (PA04). Fig. 5b showed that at constant feed pressure, water permeance and salt rejection decreased with salt concentration.

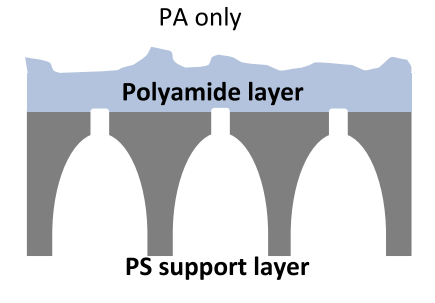
The effect of N-GOQD concentration on PA structure has been shown schematically in Fig. 6. Initial increase of N-GOQD concentration in MPD solution leads to incorporation of N-GOQD nanoparticles into PA layer and subsequent increase of the surface roughness as well as affective surface area. Different active groups, such as carboxylic acid, epoxy and hydroxyl groups, on N-GOQD surface allow a thin layer of PA to grow around the nanoparticles. Presence of more N-GOQD nanoparticles on the surface of PA can create a uniform layer of PA and change the surface morphology from leaf-like to hill and valley. In the high concentration of N-GOQD nanoparticles, more nanoparticles stick together and form an agglomerated nanoparticle in the PA matrix. Moreover, those nanoparticles decrease diffusion rate of monomers and IP reaction zone, therefore PA layer can grow around N-GOQD nanoparticles and create a fully hill and valley morphology.

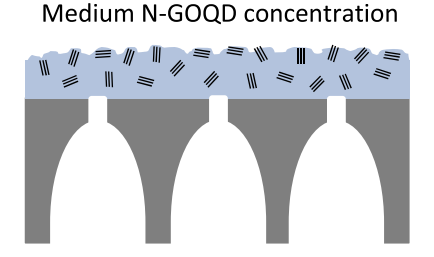
4. Conclusion

N-GOQD was prepared by a low-cost, bottom-up method and utilized as an effective additive to greatly improve desalination performance of PA TFN membranes. Different from other physically added additives, N-GOQD participated into the IP reaction and formed a crosslinked polymeric matrix with PA. Both membrane surface properties (surface hydrophilicity and effective surface area) and internal local membrane structure were modified. Compared with PA, at the optimum N-GOQD loading 0.1 w/v% TMC, 2 w/v% MPD and 0.02 to 0.04 w/v% N-GOODs. PA TFN membrane became more thermally stable, apparently resulting from the improved crosslinking between N-GOOD and the PA matrix. PA02 also showed improved hydrophilicity, as indicated by the smaller water contact angle, and higher effective surface area. As a result, the best TFN membrane in this study, showed an approximately 3-time increase of water permeability while maintaining similar salt rejection. N-GOQD, therefore, may be a promising additive to prepare high flux PA TFN membranes for desalination.

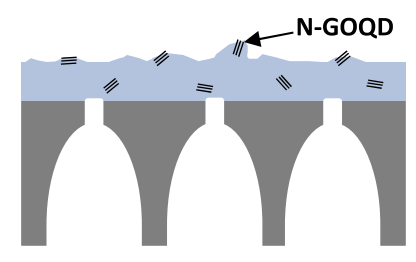
Acknowledgements

We gratefully acknowledge the support by National Science Foundation (NSF) Career Award under Grant No. 1451887.





Low N-GOQD concentration



High N-GOQD concentration

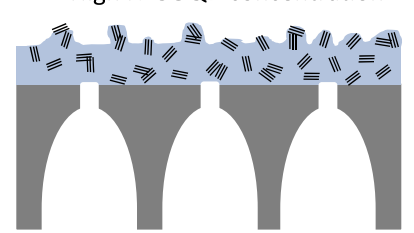


Fig. 6. Schematics showing incorporation of N-GOQD with different concentrations into TFN membrane.

Appendix A. Supplementary data

Supplementary data to this article can be found online at http://dx.doi.org/10.1016/j.desal.2017.07.014.

References

- M. Fathizadeh, A. Aroujalian, A. Raisi, Preparation and characterization of thin film composite reverses osmosis membranes with wet and dry support layer, Desalin. Water Treat. 56 (2015) 2284–2295.
- [2] A. Soroush, J. Barzin, M. Barikani, M. Fathizadeh, Interfacially polymerized polyamide thin film composite membranes: preparation, characterization and performance evaluation. Desalination 287 (2012) 310–316.
- [3] M. Fathizadeh, W.W.L. Xu, F.L. Zhou, Y. Yoon, M. Yu, Graphene oxide: a novel 2dimensional material in membrane separation for water purification, Adv. Mater. Interfaces 4 (2017)
- [4] M. Fathizadeh, A. Aroujalian, A. Raisi, Effect of lag time in interfacial polymerization on polyamide composite membrane with different hydrophilic sub layers, Desalination 284 (2012) 32–41.
- [5] J.G. Zhang, Z.W. Xu, W. Mai, C.Y. Min, B.M. Zhou, M.J. Shan, Y.L. Li, C.Y. Yang, Z. Wang, X.M. Qian, Improved hydrophilicity, permeability, antifouling and mechanical performance of PVDF composite ultrafiltration membranes tailored by oxidized low-dimensional carbon nanomaterials, J. Mater. Chem. A 1 (2013) 3101–3111
- [6] M. Fathizadeh, A. Aroujalian, A. Raisi, Effect of added NaX nano-zeolite into polyamide as a top thin layer of membrane on water flux and salt rejection in a reverse osmosis process, J. Membr. Sci. 375 (2011) 88–95.
- [7] S.H. Kim, S.Y. Kwak, B.H. Sohn, T.H. Park, Design of TiO₂ nanoparticle self-assembled aromatic polyamide thin-film-composite (TFC) membrane as an approach to solve biofouling problem, J. Membr. Sci. 211 (2003) 157–165.
- [8] G.L. Jadav, V.K. Aswal, P.S. Singh, SANS study to probe nanoparticle dispersion in nanocomposite membranes of aromatic polyamide and functionalized silica nanoparticles, J. Colloid Interface Sci. 351 (2010) 304–314.
- [9] S. Inukai, R. Cruz-Silva, J. Ortiz-Medina, A. Morelos-Gomez, K. Takeuchi, T. Hayashi, A. Tanioka, T. Araki, S. Tejima, T. Noguchi, M. Terrones, M. Endo, High-performance multi-functional reverse osmosis membranes obtained by carbon nanotube polyamide nanocomposite, Sci Rep 5 (2015).
- [10] J. Yin, G.C. Zhu, B.L. Deng, Graphene oxide (GO) enhanced polyamide (PA) thinfilm nanocomposite (TFN) membrane for water purification, Desalination 379 (2016) 93–101.
- [11] S. Bano, A. Mahmood, S.J. Kim, K.H. Lee, Graphene oxide modified polyamide nanofiltration membrane with improved flux and antifouling properties, J. Mater. Chem. A 3 (2015) 2065–2071.
- [12] M. Safarpour, A. Khataee, V. Vatanpour, Thin film nanocomposite reverse osmosis membrane modified by reduced graphene oxide/TiO₂ with improved desalination performance, J. Membr. Sci. 489 (2015) 43–54.
- [13] W.S. Hummers, R.E. Offeman, Preparation of graphitic oxide, J. Am. Chem. Soc. 80 (1958) 1339.
- [14] J.R. Lomeda, C.D. Doyle, D.V. Kosynkin, W.F. Hwang, J.M. Tour, Diazonium functionalization of surfactant-wrapped chemically converted graphene sheets, J. Am. Chem. Soc. 130 (2008) 16201–16206.
- [15] W. Choi, J. Choi, J. Bang, J.H. Lee, Layer-by-layer assembly of graphene oxide nanosheets on polyamide membranes for durable reverse-osmosis applications, ACS Appl. Mater. Interfaces 5 (2013) 12510–12519.

- [16] H. Li, Z.N. Song, X.J. Zhang, Y. Huang, S.G. Li, Y.T. Mao, H.J. Ploehn, Y. Bao, M. Yu, Ultrathin, molecular-sieving graphene oxide membranes for selective hydrogen separation, Science 342 (2013) 95–98.
- [17] Y. Huang, H. Li, L. Wang, Y.L. Qiao, C.B. Tang, C.I. Jung, Y.M. Yoon, S.G. Li, M. Yu, Ultrafiltration membranes with structure-optimized graphene-oxide coatings for antifouling oil/water separation, Adv. Mater. Interfaces 2 (2015).
- [18] X.L. Zhan, G.F. Zhang, X. Chen, R. He, Q.H. Zhang, F.Q. Chen, Improvement of antifouling and antibacterial properties of poly(ether sulfone) UF membrane by blending with a multifunctional comb copolymer, Ind. Eng. Chem. Res. 54 (2015) 11312–11318.
- [19] W. Jang, J. Yun, K. Jeon, H. Byun, PVdF/graphene oxide hybrid membranes via electrospinning for water treatment applications, RSC Adv. 5 (2015) 46711–46717.
- [20] C.Q. Zhao, X.C. Xu, J. Chen, F.L. Yang, Optimization of preparation conditions of poly(vinylidene fluoride)/graphene oxide microfiltration membranes by the Taguchi experimental design, Desalination 334 (2014) 17–22.
- [21] S.G. Kim, D.H. Hyeon, J.H. Chun, B.H. Chun, S.H. Kim, Novel thin nanocomposite RO membranes for chlorine resistance, Desalin. Water Treat. 51 (2013) 6338–6345.
- [22] H.R. Chae, J. Lee, C.H. Lee, I.C. Kim, P.K. Park, Graphene oxide-embedded thin-film composite reverse osmosis membrane with high flux, anti-biofouling, and chlorine resistance, J. Membr. Sci. 483 (2015) 128–135.
- [23] J. Shen, Y. Zhu, X. Yang, C. Li, Graphene quantum dots: emergent nanolights for bioimaging, sensors, catalysis and photovoltaic devices, Chem. Commun. 48 (2012) 3686–3699.
- [24] H.P. Cong, J.F. Chen, S.H. Yu, Graphene-based macroscopic assemblies and architectures: an emerging material system, Chem. Soc. Rev. 43 (2014) 7295–7325.
- [25] M. Nurunnabi, Z. Khatun, K.M. Huh, S.Y. Park, D.Y. Lee, K.J. Cho, Y.K. Lee, In vivo biodistribution and toxicology of carboxylated graphene quantum dots, ACS Nano 7 (2013) 6858–6867.
- [26] C.Y. Wu, C. Wang, T. Han, X.J. Zhou, S.W. Guo, J.Y. Zhang, Insight into the cellular internalization and cytotoxicity of graphene quantum dots, Adv. Healthc. Mater. 2 (2013) 1613–1619.
- [27] Z. Zeng, D. Yu, Z. He, J. Liu, F.-X. Xiao, Y. Zhang, R. Wang, D. Bhattacharyya, T.T.Y. Tan, Graphene oxide quantum dots covalently functionalized PVDF membrane with significantly-enhanced bactericidal and antibiofouling performances, Sci Rep 6 (2016).
- [28] Y. Zhang, H. Gao, J.J. Niu, B.T. Liu, Facile synthesis and photoluminescence of graphene oxide quantum dots and their reduction products, New J. Chem. 38 (2014) 4970–4974.
- [29] N.T. Ho, H.N. Tien, S.J. Jang, V. Senthilkumar, Y.C. Park, S. Cho, Y.S. Kim, Enhancement of recombination process using silver and graphene quantum dot embedded intermediate layer for efficient organic tandem cells, Sci Rep 6 (2016).
- [30] S.J. Zhu, J.H. Zhang, C.Y. Qiao, S.J. Tang, Y.F. Li, W.J. Yuan, B. Li, L. Tian, F. Liu, R. Hu, H.N. Gao, H.T. Wei, H. Zhang, H.C. Sun, B. Yang, Strongly green-photo-luminescent graphene quantum dots for bioimaging applications, Chem. Commun. 47 (2011) 6858–6860.
- [31] X.L. Li, H.L. Wang, J.T. Robinson, H. Sanchez, G. Diankov, H.J. Dai, Simultaneous nitrogen doping and reduction of graphene oxide, J. Am. Chem. Soc. 131 (2009) 15939–15944.
- [32] L. Wang, Y.L. Wang, T. Xu, H.B. Liao, C.J. Yao, Y. Liu, Z. Li, Z.W. Chen, D.Y. Pan, L.T. Sun, M.H. Wu, Gram-scale synthesis of single-crystalline graphene quantum dots with superior optical properties, Nat. Commun. 5 (2014).
- [33] Y. Wang, Y.Y. Shao, D.W. Matson, J.H. Li, Y.H. Lin, Nitrogen-doped graphene and its application in electrochemical biosensing, ACS Nano 4 (2010) 1790–1798.
- [34] C.F. Hu, Y.L. Liu, Y.H. Yang, J.H. Cui, Z.R. Huang, Y.L. Wang, L.F. Yang, H.B. Wang, Y. Xiao, J.H. Rong, One-step preparation of nitrogen-doped graphene quantum dots from oxidized debris of graphene oxide, J. Mater. Chem. B 1 (2013) 39–42.

[35] B.H. Jeong, E.M.V. Hoek, Y.S. Yan, A. Subramani, X.F. Huang, G. Hurwitz, A.K. Ghosh, A. Jawor, Interfacial polymerization of thin film nanocomposites: a new concept for reverse osmosis membranes, J. Membr. Sci. 294 (2007) 1–7.

- [36] M.L. Lind, A.K. Ghosh, A. Jawor, X.F. Huang, W. Hou, Y. Yang, E.M.V. Hoek, Influence of zeolite crystal size on zeolite-polyamide thin film nanocomposite membranes, Langmuir 25 (2009) 10139–10145.
- [37] J.M. Arsuaga, A. Sotto, G. del Rosario, A. Martinez, S. Molina, S.B. Teli, J. de Abajo, Influence of the type, size, and distribution of metal oxide particles on the properties of nanocomposite ultrafiltration membranes, J. Membr. Sci. 428 (2013) 131–141.
- [38] P.S. Goh, A.F. Ismail, B.C. Ng, Carbon nanotubes for desalination: performance evaluation and current hurdles, Desalination 308 (2013) 2–14.
- [39] B. Rajaeian, A. Rahimpour, M.O. Tade, S.M. Liu, Fabrication and characterization of polyamide thin film nanocomposite (TFN) nanofiltration membrane impregnated with TiO₂ nanoparticles, Desalination 313 (2013) 176–188.
- [40] Z. Yang, J. Yin, B.L. Deng, Enhancing water flux of thin-film nanocomposite (TFN) membrane by incorporation of bimodal silica nanoparticles, AIMS Environ. Sci. 3 (2016) 185–198.
- [41] S. Karan, Z.W. Jiang, A.G. Livingston, Sub-10 nm polyamide nanofilms with ultrafast solvent transport for molecular separation, Science 348 (2015) 1347–1351.

- [42] I. Sadeghi, A. Aroujalian, A. Raisi, M. Fathizadeh, B. Dabir, Effect of solvent, hydrophilic additives and corona treatment on performance of polyethersulfone UF membranes for oil/water separation, Procedia Eng. 44 (2012) 1539–1541.
- [43] I. Sadeghi, A. Aroujalian, A. Raisi, B. Dabir, M. Fathizadeh, Surface modification of polyethersulfone ultrafiltration membranes by corona air plasma for separation of oil/water emulsions, J. Membr. Sci. 430 (2013) 24–36.
- [44] A. Kovalchuk, K.W. Huang, C.S. Xiang, A.A. Marti, J.M. Tour, Luminescent polymer composite films containing coal-derived graphene quantum dots, ACS Appl. Mater. Interfaces 7 (2015) 26063–26068.
- [45] S.Y. Kwak, S.G. Jung, Y.S. Yoon, D.W. Ihm, Details of surface features in aromatic polyamide reverse osmosis membranes characterized by scanning electron and atomic force microscopy, J. Polym. Sci. Polym. Phys. 37 (1999) 1429–1440.
- [46] G. Hurwitz, G.R. Guillen, E.M.V. Hoek, Probing polyamide membrane surface charge, zeta potential, wettability, and hydrophilicity with contact angle measurements, J. Membr. Sci. 349 (2010) 349–357.
- [47] M.N. Abu Seman, M. Khayet, N. Hilal, Nanofiltration thin-film composite polyester polyethersulfone-based membranes prepared by interfacial polymerization, J. Membr. Sci. 348 (2010) 109–116.